buildings

Article

Prediction of the Debonding Failure of Beams Strengthened with FRP through Machine Learning Models

Tianyu Hu [1,2], Hong Zhang [1,2,*] and Jianting Zhou [1,2]

1 State Key Laboratory of Mountain Bridge and Tunnel Engineering, Chongqing Jiaotong University, Chongqing 400074, China
2 School of Civil Engineering, Chongqing Jiaotong University, Chongqing 400074, China
* Correspondence: hongzhang@cqjtu.edu.cn

Abstract: Plate end (PE) debonding and intermediate crack (IC) debonding are the two main failure modes of beams strengthened with fiber-reinforced polymer (FRP) in flexure. Therefore, it is essential to clarify the force state of the structure when debonding occurs in strengthened beams. This paper collected 229 beams with debonding failure as the database, of which 128 were PE debonding and 101 were IC debonding. Correlation and grey correlation analysis were used to establish the indicator systems for predicting PE and IC debonding and to identify the critical indicators among them. Five machine learning models, linear regression, ridge regression, decision trees, random forests, and back propagation (BP) neural networks, were used to build the two debonding prediction models. Optimization of the best prediction among the five machine learning models took place using the Dung Beetle Optimizer (DBO) algorithm, which has competitive performance with state-of-the-art optimization approaches in terms of convergence rate, solution accuracy, and stability. Finally, the optimal prediction model was compared with the models suggested by codes, and it was found that the established model can well predict PE and IC debonding.

Keywords: plate end debonding; intermediate crack debonding; fiber-reinforced polymer; machine learning; dung beetle optimizer (DBO)

check for updates

Citation: Hu, T.; Zhang, H.; Zhou, J. Prediction of the Debonding Failure of Beams Strengthened with FRP through Machine Learning Models. *Buildings* **2023**, *13*, 608. https://doi.org/10.3390/buildings13030608

Academic Editor: Krishanu Roy

Received: 29 January 2023
Revised: 21 February 2023
Accepted: 24 February 2023
Published: 25 February 2023

1. Introduction

In recent years, deformation and strengthening of structures have been widely studied [1–4]; fiber-reinforced polymers (FRP) have been widely used to strengthen structures [5]. However, due to the linear elasticity of the material, debonding failure occurs in FRP-strengthened reinforced concrete (RC) beams before the FRP has reached its full performance, which largely limits its further application. [6–10]. PE and IC debonding are the two failure modes for FRP-strengthened RC beams (Figure 1). Generally, IC debonding occurs in beams with a relatively large shear-span-to-depth ratio, while for beams with a relatively small shear-span-to-depth ratio, since the bending moment is minor at this time, the beams are mainly subjected to shear strength, so PE debonding occurs [6]. Nevertheless, due to the complex mechanism of debonding failure of FRP-strengthened RC beams in flexure, it is not realistic to judge the failure modes in strengthened beams merely by shear-span-to-depth ratio [11,12].

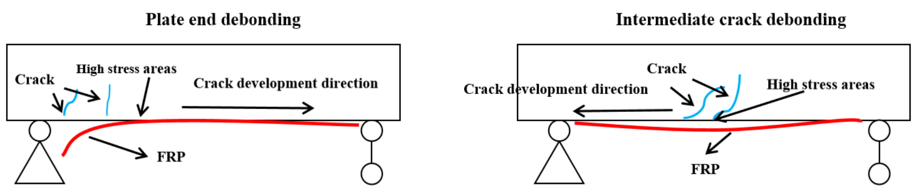

Figure 1. Debonding modes.

To clarify the failure mechanism of FRP-strengthened RC beams, researchers have conducted a lot of experiments and proposed some models. For PE debonding, in 1992, Oehlers proposed a model for strength based on the forces of shear and flexural moments which act on the end of the plate [11]. In 1997, Jansze proposed a plate-end debonding strength model for steel-plated beams. The model focuses on PE debonding of the strengthened beams at the onset of shear cracking [13]. Ahmed and Van Germert, in 1999, modified Jansze's model to take into account the differences between FRP and steel properties and the effect of shear reinforcement [14]. In 2001, fib Bulletin adopted Blaschko's beam-based model for the shear strength of concrete [15]. In 2002, Smith and Teng proposed a concrete shear strength model for PE debonding [16]. Yao and Teng, in 2007, conducted tests on FRP-strengthened RC beams and modified the expressions proposed by Oehlers [17]. TR55 in 2012, ACI and AS in 2017 recommended an upper limit on the shear force in the plate end region to avoid PE debonding [18–20]. El-Sayed proposed a model for predicting PE debonding based on the beam's concrete shear strength, which considers the parameters that affect the opening of shear cracks in 2021 [21]. For IC debonding, in 2001, fib and JSCE proposed models which limit the tensile stress during debonding [15,22]. CECS 2003, CNR 2004, and TR55 2012 present FRP ultimate debonding strain models which are based on tests of shear at the interface between FRP and concrete. [18,23,24]. In 2013, Kim and Harries proposed a Monte Carlo prediction model for the effective strain of FRP based on the statistical approach [25]. Bilotta et al., in 2013, proposed standard and design values for the maximum tensile strain of FRP when IC debonding occurs based on flexural tests of RC beams strengthened with FRP [26]. In 2016, Lopez-Gonzalez characterized the FRP–concrete interface of the strengthened beams and proposed an interface fracture energy model [27]. ACI modified the model proposed by Teng in 2003 based on the maximum tensile strain of RC beams strengthened with FRP and proposed a model for calculating the allowable debonding strain of FRP in 2017 [20]. Li and Wu investigated the mechanism of IC debonding of FRP-strengthened beams using a finite element analysis model based on the smeared-crack method in 2018. They established a model for IC debonding based on the finite element analysis simulation results [28].

These models for predicting PE and IC debonding have facilitated the study of the debonding failure of FRP-strengthened RC beams. Still, they have significant coefficients of variation between the calculated and experimental values [21,29]. Therefore, it is necessary to conduct a deeper study on debonding failure to establish more accurate models for predicting PE and IC debonding. In recent years, machine learning has been widely used in structural engineering [30–32]. In this paper, a data-driven model was adopted, which reduces the cost of experiments and is scientific in the selection of indicators; 229 beams with debonding failure were collected as a database, of which 128 were PE debonding and 101 were IC debonding. Correlation analysis and grey correlation analysis were used to establish the indicator systems for predicting PE and IC debonding and to identify the important indicators among them. Five machine learning models, linear regression, ridge regression, decision trees, random forests, and BP neural networks, were used to build the two debonding prediction models. Optimization of the best prediction among the five machine learning models took place using the Dung Beetle Optimizer (DBO). Finally, the optimal prediction model was compared with the models suggested by codes.

2. Construct the Indicator System

2.1. Primary Indicator System

Based on the relevant codes and experimental studies [6–8,10–12,25–32], in the primary indicator system, according to the literature [18–24], as shown in Figure 2, independent indicators and mixed indicators systems are constructed, respectively. Among them, the mixed indicator is a linear combination of independent indicators. The combination principle is based on the codes and related literature [16–24]. In contrast, the independent indicator system is the physical composition of the study object itself, including the geometric and material properties of the reinforced material itself and the geometric and material properties of the reinforced material.

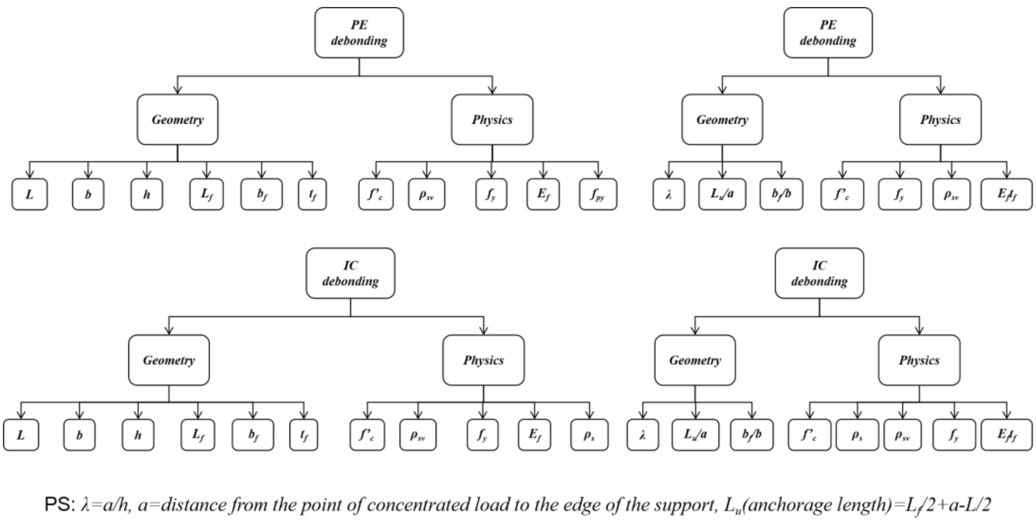

Figure 2. Primary indicator system.

2.2. Data Collection

The data collection criteria are as follows:

(a) Debonding failure occurred in all 229 strengthened beams, including IC debonding and PE debonding, as shown in Table 1.
(b) The FRP sheets were not prestressed. The ends of the strengthened beams were not anchored.
(c) The geometric and material properties of the strengthened beams, FRP, and reinforcements are clear.

Table 1. Data sources and failure modes.

Reference	Beam	Number	Failure Mode
[33]	C D G I M	5	PE
[34]	B2 B3 B4 B6	4	PE
[35]	A4 A5 B3	3	PE
[36]	1Bu 2Bu 3Bu 1Cu 2Cu 3Cu	6	PE
[37]	B1U,1.0 B3U,1.0 B4U,1.0 B1U,2.3	4	PE
[38]	VR5 VR6 VR7 VR8	4	PE
[39]	P2 P3 P4 P5	4	PE
[40]	2	1	PE
[41]	A3 A8 C2	3	PE
[42]	AF.2 AF.2.1 AF.3 AF.4 BF.2-1 BF.3-1 CF.2-1 CF.3-1	15	PE
	CF.4-1 DF2 DF3 DF4 EF.1-1 EF.3-1 EF.4-1		PE
[43]	BF2 BF3 BF4 BF5	4	PE
[44]	F5 F6 F7 F10	4	PE
[45]	1N4 1N6	2	PE
[46]	Beam3 Beam4 Beam5	3	PE
[47]	A950 A1100 A1150	3	PE
[48]	A4 A6 A8 B5	4	PE
[49]	1A 1B 2A 2B 3A 3B	6	PE
[50]	A-S1 B-S1	2	PE
[51]	A1-1 A2-1 A3-1 A4-1 A5-1	10	PE
	A1-11 A2-11 A3-11 A4-11 A5-11		PE
[52]	1T6LN 2T6LN 2T4LN	3	PE
[53]	A0 B0	2	PE

Table 1. *Cont.*

Reference	Beam	Number	Failure Mode
[54]	Bb1 Bb3	2	PE
[55]	E1a E1b E2a E2b E3a E3b	11	PE
	E4a E4b E5a E5b E3b2		PE
[56]	RB1	1	PE
[57]	B3-12D-2L15 B4-12D-3L15	2	PE
[17]	CS-B CS-L3-B CS-W100-B CP-B	4	PE
[58]	A3 B2 B3	3	PE
[59]	B85P B70P B25P	3	PE
[60]	C2	1	PE
[10]	S-0.5-35-360	1	PE
[61]	S(AT1)C B(AT1)C	2	PE
[62]	BC1-1 BC1-2 BC2-1 BC3-1 BC4-1 BC4-2	6	PE
[55]	B	1	IC
[6]	SM2 SM3 MM2 MM3	4	IC
[63]	A1.1 A3.1	2	IC
[64]	S-A R-A	2	IC
[65]	H-75-2 C3	2	IC
[66]	CB3-2S CB4-2S CB5-3S CB6-3S	8	IC
	CB7-1S CB8-1SB CB9-1SB CB10-2SB		IC
[67]	A11 A12 A21 A31 A32	9	IC
[68]	A41 A42 A51 A52		IC
[51]	BP BF	2	IC
	A3 A4 A5 A6 B3 B4 B5 B6	8	IC
[54]	A10 A20 B10 B20	4	IC
[69]	S1a S1b S2a S2b S3a S3b	6	IC
[70]	B11 B12 B21 B22 B31 B32	6	IC
	Beam 2 Beam 6	2	IC
[71]	S2PF7M S3PS1M S3PS2M	3	IC
[72]	B5 B6 B7 B8	4	IC
[73]	A2	1	IC
	NFCB1 NFCBW2	2	IC
[74]	EBR	1	IC
[58]	1 2 4 3 9	10	IC
[75]	10 11 12 5 6		IC
	B-04/0.5S B-08/S1 BF-04/0.5S BF-06/S	4	IC
[76]	S-0 S-0.4 S-0.6	3	IC
[77]	W-CSP1-0 W-CSP1-0E W-CSP1-4(1) W-CSP2-3-0	17	IC
[78]	W-CSP2-3-4(1) W-CSP2-3-4(2) W-CSP2-3-4(3)		
	W-CSP6-9-0 W-CSP6-9-4(1) W-CSP6-9-4(2) W-CSP6-9-4(3)		
	P-CSP1(1) P-CSP2-3(1) P-CSP2-3(2) P-CSP6-9(1) P-CSP6-9(2)		

The range of the parameters is large, which includes the general situation in practical applications.

2.3. Data Analysis and Indicator System Establishment

There are many independent indicators affecting PE and IC debonding of the strengthened beams and it is unclear whether there is a relationship between each independent indicator and the debonding failure, so correlation and grey correlation analysis were used to identify the redundant indicators.

2.3.1. Correlation Analysis

The correlation between the indicators is expressed by Pearson correlation coefficient, with a correlation coefficient close to 1 for a positive correlation and close to −1 for a negative correlation [79]. The formula for its calculation is given in Equation (1).

$$r_{xy} = \frac{Cov(X,Y)}{S_x S_y} \tag{1}$$

where $Cov(x,y) = \frac{\sum_{1}^{n}(X_i - X).(Y_i - Y)}{n-1}$, $S_x = \sqrt{\frac{\sum_{1}^{n}(X_i - \overline{X})^2}{n-1}}$ and $Cov(x,y)$ denotes the covariance of x and y, S_x denotes the standard deviation of variable x, and S_y denotes the standard deviation of variable y

The correlation coefficients (expressed as P) between independent indicators were calculated as shown in Figure 3. In it, the absolute value of the correlation coefficient of the indicator is compared with 0.5, and the correlation between indicators is strong if it is greater than 0.5 and the correlation is weak if it is less than 0.5.

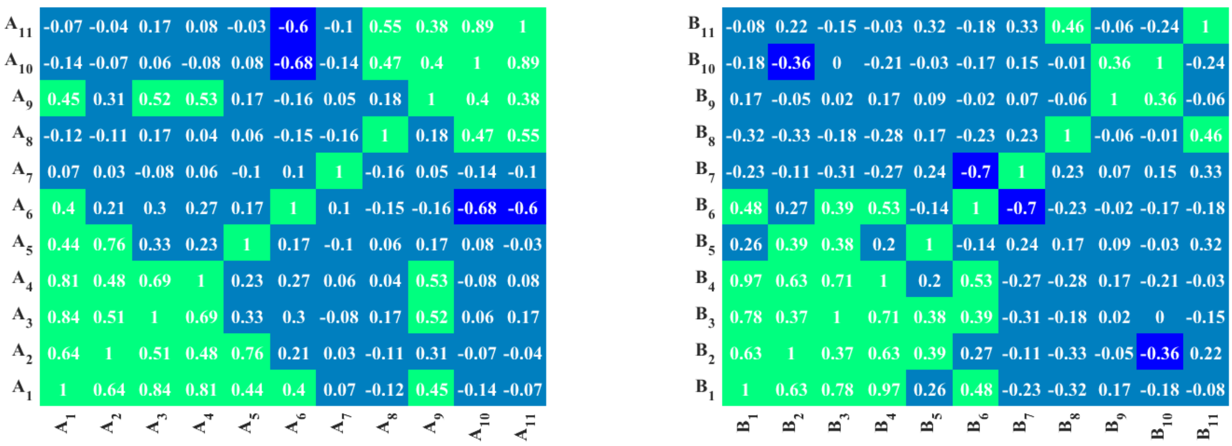

Figure 3. p-value of independent indicators of PE and IC failure.

In Figure 3, A_1 to A_{11} are L, b, h, L_f, b_f, t_f, f'_c, ρ_{sv}, f_y, E_f, f_{py}; B_1 to B_{11} are L, b, h, L_f, b_f, t_f, f'_c, ρ_{sv}, f_y, E_f, ρ_s. It can be seen from Figure 3 that there is a significant correlation between A_1 and A_2, A_3, A_4, a significant correlation between A_2 and A_3, A_5, a significant correlation between A_3 and A_2, A_4, A_9, a significant correlation between A_4 and A_1, A_3, A_9, a significant correlation between A_5 and A_2, a significant correlation between A_6 and A_{10}, A_{11}, a significant correlation between A_8 and A_{11}, a significant correlation between A_9 and A_3, A_4, a significant correlation between A_{10} and A_6, and a significant correlation between A_{11} and A_6. Additionally, there is a significant correlation between B_1 and B_2, B_3, and B_4, a significant correlation between B_2 and B_1 and B_4, a significant correlation between B_3 and B_1 and B_4, a significant correlation between B_4 and B_1, B_2, B_3, and B_6, and a significant correlation between B_6 and B_7. In summary, the correlations among the independent indicators of PE failure are complicated, and most have significant correlations; the relationships among some indicators of IC failure are complicated and cannot be eliminated; therefore, mixed indicators are considered in establishing the indicator system. The correlation analysis results of the mixed indicators are shown in Figure 4.

In Figure 4, a_1 to a_7 are λ, L_u/a, b_f/b, f'_c, f_y, ρ_{sv}, $E_f t_f$; b_1 to b_8 are λ, L_u/a, b_f/b, f'_c, ρ_s, ρ_{sv}, f_y, $E_f t_f$. It can be seen from Figure 4 that the mixed indicators of PE failure indicators are weakly or lowly correlated (because the P-value between these indicators are less than 0.5), and no indicators need to be removed; the mixed indicators of IC failure are all weakly or lowly correlated with each other also, and as with PE failure, there is no need to eliminate any indicator.

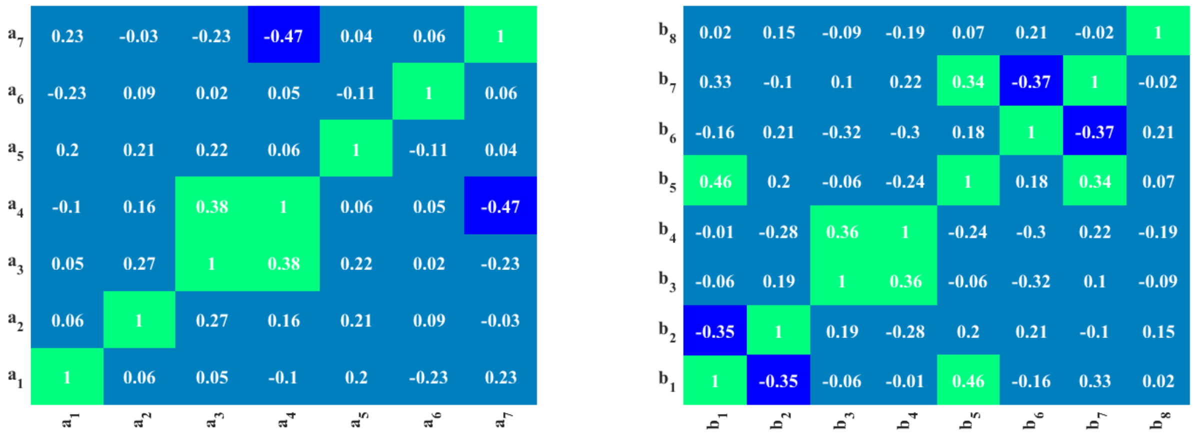

Figure 4. *p*-value of mixed indicators of PE and IC failure.

2.3.2. Grey Correlation Analysis

Grey correlation analysis is used to determine the degree of influence of each factor on the system [80]. The basic steps are as follows.

(a) Determine the reference series reflecting the characteristics of the system behavior and the comparison series affecting the system behavior.
(b) Dimensionless processing of the reference and comparison series.
(c) Find the grey correlation coefficient between the reference series and the comparison series, noted here as ξ, which is shown in Equation (2).

$$\xi(x_0(k), x_i(k)) = \frac{a + \rho b}{|x_0(k) - x_i(k)| + \rho b}, \forall i, k \tag{2}$$

where a denotes the minimum difference of the data in the subsequence and b denotes the maximum difference of the data in the subsequence; ρ is the resolution factor and generally taken as 0.5.

(d) Search for correlation. Because the correlation coefficient is the value of the degree of correlation between the comparison series and the reference series at each point, it has more than one number, and the information is too scattered to facilitate a holistic comparison. Therefore, it is necessary to pool the correlation coefficients at each point into one value; that is, to find its average value, as a quantitative representation of the degree of correlation between the comparison series and the reference series, the correlation degree is noted as r_i, and its formula is as follows in Equation (3).

$$r_i = \frac{1}{N} \sum_{k=1}^{N} \xi_i(k) \tag{3}$$

The grey correlation of each indicator of PE and IC with failure is shown in Figure 5.

From Figure 5, it can be seen that the degree of the influence of the parameters on PE debonding are FRP stiffness (Eftf), concrete strength (f'c), the ratio of sheet width to beam width (bf/b), stirrup reinforcement ratio (ρsv), tensile strength of tensile reinforcement (fy), shear span ratio (λ), and location of FRP cut-off point (Lu/a); the output parameter is the shear strength ($V_{db,end}$). As for IC debonding, the degree of influence of the parameters on it are concrete strength (f'c), FRP stiffness (Eftf), shear span ratio (λ), stirrup reinforcement ratio (ρsv), the ratio of sheet width to beam width (bf/b), tensile strength of tensile reinforcement (fy), tensile reinforcement ratio (ρs), and location of FRP cut-off point (Lu/a); the output parameter is the debonding strain of FRP (ε_{fd}). It can be obtained that FRP stiffness (Eftf) and concrete strength (f'c) have a large effect on both PE and IC debonding and this conclusion is roughly the same as the models suggested by codes [15,18–20,22–24].

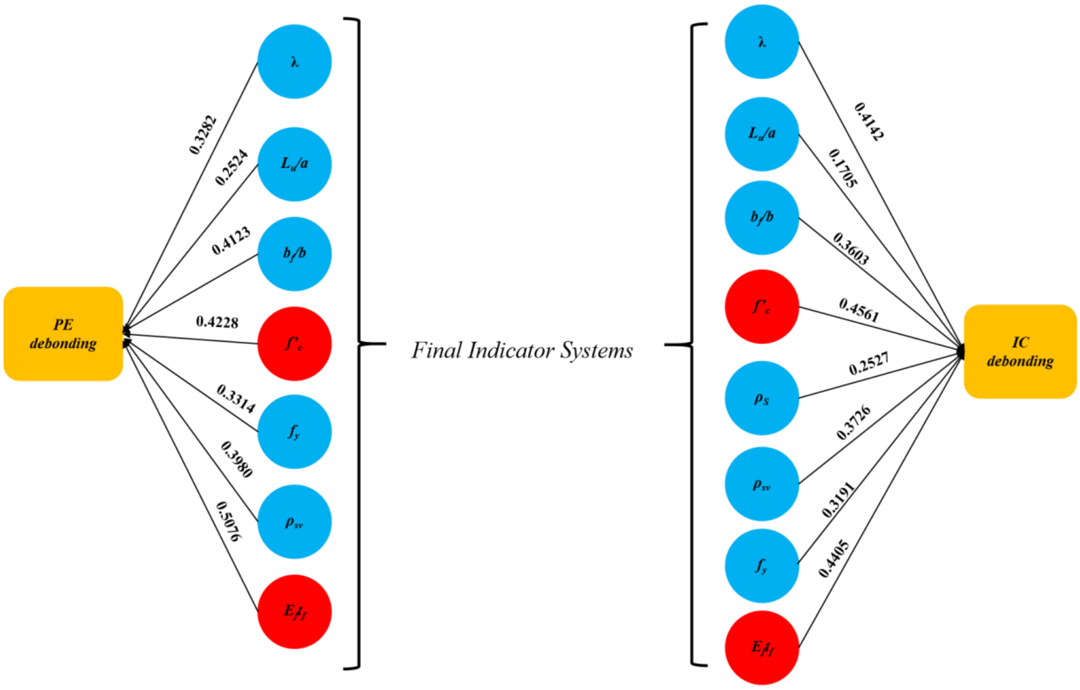

Figure 5. Indicator systems of the debonding failure.

3. Construction of the Machine Learning Models

3.1. Machine Learning Algorithms

3.1.1. Linear Regression

Linear regression (LR) can be classified as univariate linear regression, and multivariate linear regression, which establishes a functional relationship between the dependent and independent variables and is a supervised machine learning algorithm [81]. This paper uses multivariate linear analysis because of the large number of independent variables. Its expression is given in Equation (4).

$$Y = \beta 0 + \sum_{j=1}^{m} Xj\beta j \tag{4}$$

where Y denotes the dependent variable, which in this paper represents the shear force at the end of the beam when PE debonding occurs and the strain of the sheet at the middle of the beam when IC debonding occurs; β_0 is the regression constant; m denotes the number of independent variables; X_j denotes the independent variable, which in this paper is the parameter for predicting the debonding; and β_j is the regression coefficient. The root mean square error is minimized by the gradient descent method, and the best combination of regression coefficients is subsequently obtained, which in turn leads to the best-fit line.

3.1.2. Ridge Regression

The ridge regression (RR) is a modified linear regression method. By giving up the unbiased nature of linear regression, the regression method obtains more realistic and reliable regression coefficients at the cost of losing some information and accuracy, and the fit to the pathological data is stronger than that of the ordinary linear regression method [82].

3.1.3. Decision Tree

The decision tree (DT) is a classic machine learning algorithm. It mainly consists of nodes and directed edges. There are two types of nodes: the internal node and the leaf node. Internal nodes represent features or attributes, and leaf nodes represent classes or values. When the regression is performed with a decision tree, each feature of the sample is tested from the root node, and the sample is assigned to its child nodes according to the test results; at this time, each child node corresponds to one of the values taken for the feature. The samples are tested and assigned in this way recursively until they reach the leaf nodes [83].

3.1.4. Random Forest

The random forest (RF) is an algorithm that integrates multiple trees through the concept of integrated learning. Its basic unit is a decision tree, and its essence goes with an important branch of machine learning–integration learning [83]. As shown in Figure 6, from an intuitive point of view, each decision tree is a decision maker. N trees will have N decision. The random forest integrates all the decision and designates the consequence with the most decision as the final output.

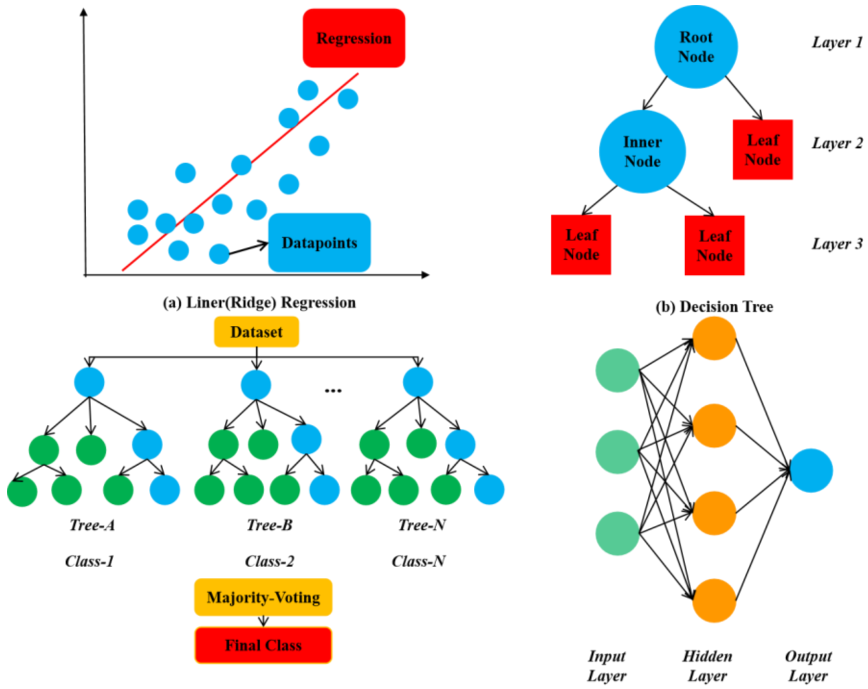

Figure 6. Architecture of the machine learning models.

3.1.5. BP Neural Network

Back propagation (BP) neural network is a multilayer forward neural network trained according to the error back propagation algorithm. Its gradient descent method is used to adjust the weights and thresholds of neurons in each layer to reduce the error of the network output. BP neural networks can achieve arbitrary nonlinear mapping of input and output, and have the characteristics of self-learning and simple structure [84].

The general architecture of the above machine learning algorithms is shown in Figure 6.

3.2. Model Construction and Evaluation

The data used for model construction were 128 sets of PE debonding and 101 sets of IC debonding, as listed in Table 1. The model's input parameters are identified in Section 2 of this paper, shown in Figure 5. For PE debonding, the input parameters are FRP stiffness ($E_f t_f$), concrete strength (f'_c), the ratio of sheet width to beam width (b_f/b), stirrup reinforcement ratio (ρ_{sv}), tensile strength of tensile reinforcement (f_y), shear span ratio (λ), and location of FRP cut-off point (L_u/a). For IC debonding, the input parameters are concrete strength (f'_c), FRP stiffness ($E_f t_f$), shear span ratio (λ), stirrup reinforcement ratio (ρ_{sv}), the ratio of sheet width to beam width (b_f/b), tensile strength of tensile reinforcement (f_y), tensile reinforcement ratio (ρ_s), location of FRP cut-off point (L_u/a). The training set, validation set, and test set of the model are 60%, 20%, and 20%, respectively.

In the paper, MAE and R^2 are used to evaluate the performance of the model, where MAE indicates the mean of the absolute error between the predicted value of the model and the actual value of the sample, and R^2 indicates the degree of fit between the predicted value of the model and the actual value of the sample, and their equation are shown in Equation (5).

$$
\begin{aligned}
MAE &= \frac{1}{n}\sum_{i=1}^{n}|y_i - p_i| \\
R^2 &= 1 - \frac{\sum_{i=1}^{n}(y_i - p_i)^2}{\sum_{i=1}^{n}(y_i - \overline{y}_i)^2}
\end{aligned}
\tag{5}
$$

where y_i is the true value of the sample, p_i is the predicted value of the model, and $\overline{y}_\mathrm{i}$ is the mean value of the sample.

The MAE and R^2 of the training set, the validation set, and the testing set of the machine learning model are shown in Figure 7; the ratio of the training, the validation, and the testing sets is 70%, 15%, and 15%. The validation set is the samples left during the model training, which can be used to adjust the hyperparameters of the model and evaluate the ability of the model. The testing set is used to evaluate the performance of the final model.

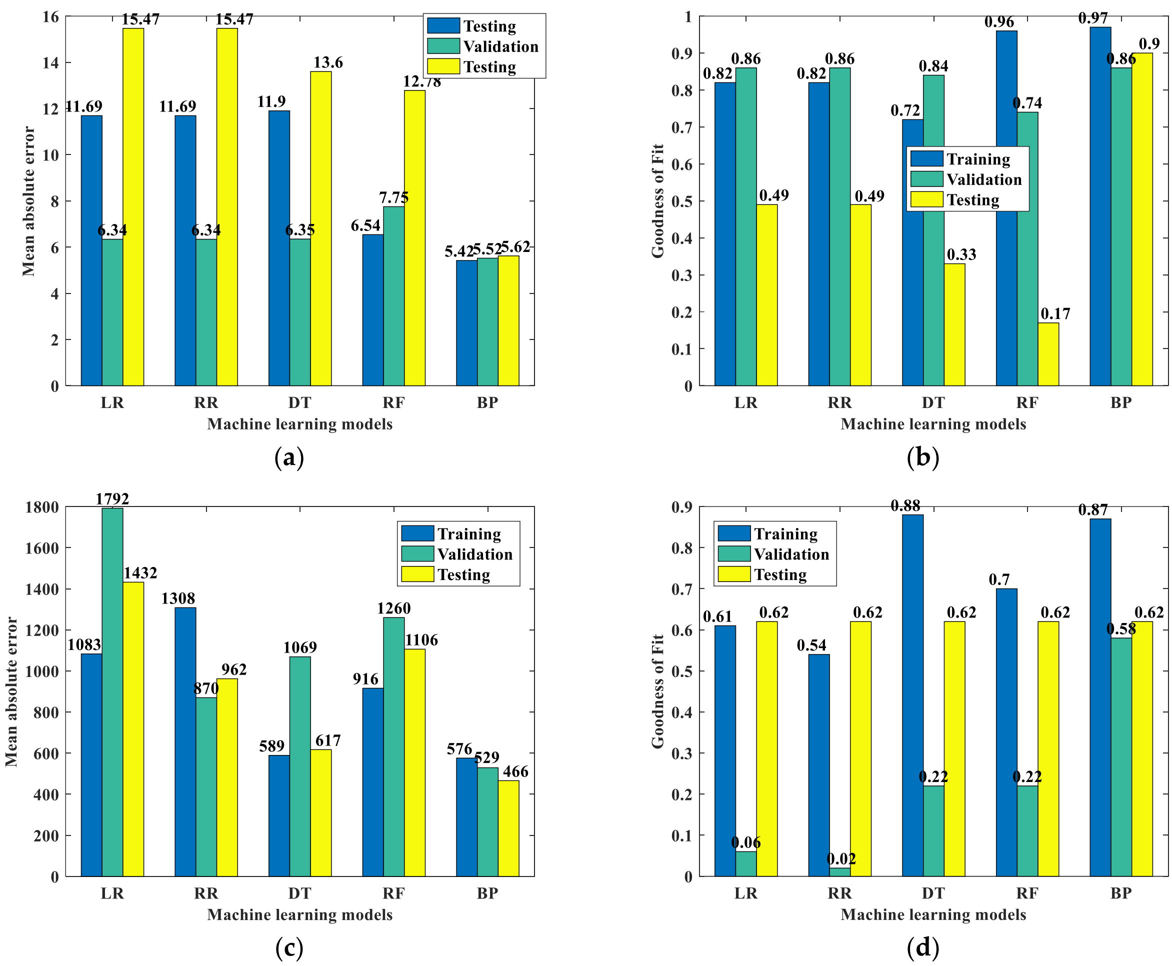

Figure 7. (**a**) MAE for PE debonding prediction model; (**b**) R^2 for PE debonding prediction model; (**c**) MAE for IC debonding prediction model; (**d**) R^2 for IC debonding prediction model.

From Figure 7a,b, it can be seen that for PE debonding, the MAE and R^2 of LR, RR, DT, and RF in the training set, the validation set, and the testing set differ significantly, indicating that the generalization ability of these models is poor, while the MAE of BP neural network in the training set, the validation set, and the testing set are 5.42, 5.52, and 5.62, respectively, which are the most minor and most average among all models. Meanwhile, the R^2 of the training set, the validation set, and the BP neural network testing set are 0.97, 0.86, and 0.90, respectively, which are also the highest among all the models. From Figure 7c,d, it can be seen that for IC debonding, the *MAE* and R^2 of LR, RR, DT, and RF in the training set, the validation set, and the testing set differ greatly, indicating that these models have poor generalization ability, while the *MAE* of BP neural network in the training set, the validation set, and the testing set are only 576, 529, and 466, respectively, which are the lowest and the most average among all models. In addition, the R^2 of the BP neural network in the training, validation, and testing sets reach 0.87, 0.58, and 0.62, respectively. Although the R^2 of the training set is lower than that of the DT, the R^2 of its validation set is higher than that of the DT. In summary, the BP neural network outperforms other machine learning models regarding prediction accuracy and debonding failure's generalization ability.

3.3. Model Optimization

For the prediction of debonding failure, it is known from Section 3.2 that the BP neural network model with the best performance still has the problem of poor generalization ability, so the BP neural network model for debonding failure prediction is considered for optimization. To overcome the shortcomings of the BP algorithm in the generation of weights and thresholds, which are easy to fall into the local optimum, and slow convergence speed, the Dung Beetle Optimizer algorithm (DBO) is used to optimize it. The Dung Beetle Optimizer algorithm is a novel swarm intelligence optimization algorithm proposed in November 2022, mainly inspired by the ball rolling, dancing, foraging, stealing, and reproduction behaviors of dung beetles and the algorithm presents substantially competitive performance with state-of-the-art optimization approaches in terms of the convergence rate, solution accuracy, and stability [85]. The coefficients of variation of the predicted and actual values of the 50 runs of DBO-BP and BP for PE and IC debonding are shown in Figure 8.

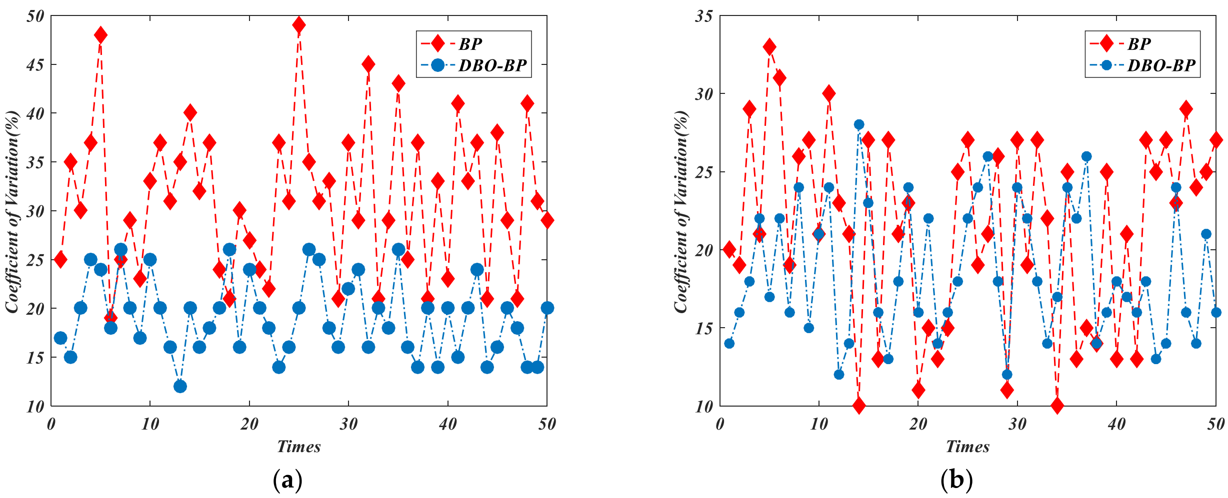

Figure 8. Comparison of model performance before and after optimization. (**a**) PE debonding; (**b**) IC debonding.

It can be seen from Figure 8 that the overall coefficient of variation of the prediction of debonding failure by the BP neural network model optimized by the DBO algorithm is smaller than that of the BP neural network model. The accuracy of the optimized model is significantly better than that of the traditional BP neural network.

4. Evaluation of Models Recommended by Codes

The models recommended by codes for PE and IC debonding are shown in Table 2. In all, 128 sets of PE debonding and 101 sets of IC debonding samples collected in 'Table 1′ are used to analyze the two types of models separately. The computed values of the models are compared with the actual values of the samples in Figure 9. The evaluation of the model is based on two indicators: coefficient of variation and conservativeness. In general, the smaller the coefficient of variation, the smaller the dispersion between the two sets of data, indicating a better predictive value of the model. The model is conservative if more than ninety percent of the predicted values are less than the test values. The performance evaluation of the codes' models is shown in Table 3.

Table 2. Models recommended by codes.

Codes	PE Debonding	IC Debonding
ACI440.2R	$V_{db,end} < 0.67V_c$	$\varepsilon_{fd} = 0.41\sqrt{\frac{f'_c}{E_f t_f}} \leq 0.9\varepsilon_{fu}$
fib	$V_{db,end} < 0.15 f_{ck}^{1/3} bd$	$\varepsilon_{fd} = \alpha c_1 k_c k_b \sqrt{\frac{f_{ct}}{E_f t_f}}$
TR55	$V_{db,end} < 0.67V_{rd}$	$\varepsilon_{fd} = 0.5k_b\sqrt{\frac{f_{ct}}{E_f t_f}}$
AS 5100.8	$V_{db,end} < 0.67V_u$	
CNR		$\varepsilon_{fd} = 0.484\sqrt{\frac{k_b\sqrt{f'_c f_{ct}}}{E_f t_f}}$
JSCE		$\varepsilon_{fd} \leq \sqrt{\frac{2G_f}{E_f t_f}}$
CECS		$\varepsilon_{fd} = k_b f_{ct}\left(\frac{1}{\sqrt{E_f t_f}} - \frac{0.2}{L_d}\right)$

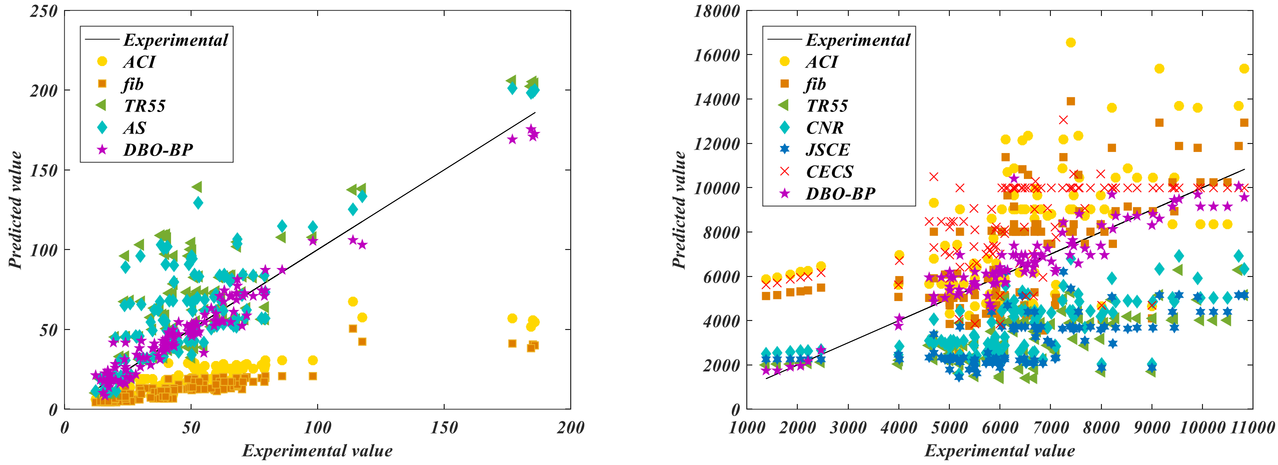

(**a**) (**b**)

Figure 9. Evaluation of the models. (**a**) PE debonding; (**b**) IC debonding.

As can be seen from Figure 9 and Table 3, for PE debonding, the models suggested by ACI and *fib* are a bit conservative, and their calculated values are lower than the experimental values. The coefficient of variation between the calculated values of the models suggested by TR55 and AS and the experimental values exceeds 40%, which is difficult to apply in practice. For IC debonding, the models suggested by TR55, CNR, and JSCE are a little conservative, while the models suggested by ACI and CECS have the risk of overestimating the FRP strains in case of the IC debonding, and the coefficients of variation between the calculated values of all the models suggested by the codes and experimental values are above 38%, which is difficult to apply in practice. For PE and IC debonding, the DBO-BP model has the lowest coefficient of variation between predicted values and experimental values among all models, which are 19% and 10%, and its predicted values are more stable, which shows a relatively balanced proportion of conservative values in the predicted values of the models.

Table 3. Model Evaluation.

	PE Debonding		**IC Debonding**	
Models	Coefficient of Variation	Conservative Value	Coefficient of Variation	Conservative Value
ACI440.2R	26.6%	100%	46.8%	29%
fib	25.1%	100%	45.4%	40%
TR55	48.3%	39%	38.6%	96%
AS 5100.8	44.5%	38%		
CNR			40.1%	94%
JSCE			44.7%	94%
CECS			38.8%	14%
DBO-BP	19%	48%	10%	42%

5. Parametric Study

The importance of the parameters is calculated based on the connection weights and excitation functions between the input layer and the hidden layer, and between the hidden layer and the output layer of the DBO-BP neural network model. In this study, the connection functions of the input layer and the hidden layer are "hyperbolic tangent function" and "linear function", which are expressed in Equations (6) and (7).

$$y_i = f \cdot \left(\sum_i w_{ij} x_i + \phi_j \right) = \frac{2}{1 + e^{-2\left(\sum_i w_{ij} x_i + \phi_j\right)}} - 1 \tag{6}$$

$$y_i = f \cdot \left(\sum_i w_{ij} x_i + \phi_j \right) = \sum_i w_{ij} x_i + \phi_j \tag{7}$$

where x_i denotes the value of the ith input metric, w_{ij} is the connection weight of the ith metric to the jth neuron, and Φ_j is the bias of the jth neuron.

The interlayer connection weights and biases for PE and IC debonding are shown in Tables 4 and 5.

The importance results of the indicators calculated according to Tables 4 and 5 are shown in Figure 10.

Table 4. Layer-to-layer connection weights for the predictive model of PE debonding.

P		***P***													
		H													**O**
		h_1	h_2	h_3	h_4	h_5	h_6	h_7	h_8	h_9	h_{10}	h_{11}	h_{12}	h_{13}	***V***
I	Φ	−0.9	−0.5	−0.3	−0.4	0.3	0.5	−0.6	1.2	−0.5	−0.4	−0.9	−0.7	−0.7	
	a_1	1.0	−0.4	−0.2	−0.9	−0.1	−0.3	−0.1	−0.2	−0.5	−0.1	0.8	0.6	0.2	
	a_2	0.8	0.4	−1.1	0.3	0.9	−1.5	0.7	0.1	0.4	0.5	−0.6	0.4	−0.1	
	a_3	−1.2	0.0	−0.3	−1.1	−0.1	0.3	−0.8	0.6	0.6	−0.1	−0.4	−0.4	−0.1	
	a_4	−0.8	0.4	−1.2	1.2	−1.1	1.7	0.0	−1.1	0.1	−0.2	−0.8	−0.7	0.4	
	a_5	0.0	−0.1	0.9	−1.6	0.7	−1.0	−0.6	0.9	0.0	−0.3	−1.2	1.3	0.4	
	a_6	0.0	1.5	−0.8	−0.2	0.5	0.7	0.8	0.6	0.2	−0.1	−1.4	0.1	−0.8	
	a_7	0.0	0.8	0.8	0.6	0.0	−0.7	−0.1	0.5	0.2	0.3	−1.0	−0.9	−0.4	

Table 4. *Cont.*

P		*P*													
		H													O
		h_1	h_2	h_3	h_4	h_5	h_6	h_7	h_8	h_9	h_{10}	h_{11}	h_{12}	h_{13}	*V*
H	Φ														0.4
	h_1														1.0
	h_2														−1.1
	h_3														0.9
	h_4														−1.5
	h_5														−0.7
	h_6														0.9
	h_7														1.3
	h_8														0.4
	h_9														0.5
	h_{10}														0.3
	h_{11}														−1.5
	h_{12}														−1.2
	h_{13}														1.3

Table 5. Layer-to-layer connection weights for the predictive model of IC debonding.

		P					
		H					O
		h_1	h_2	h_3	h_4	h_5	ε
I	Φ	−0.6	0.4	−0.3	1.1	−0.1	
	b_1	0.9	−1.2	−0.4	−0.2	−0.8	
	b_2	−0.4	−0.6	0.7	−0.6	1.0	
	b_3	−0.1	0.3	0.1	0.6	0.7	
	b_4	−0.4	0.8	1.2	−0.1	−0.8	
	b_5	−0.6	0.1	0.2	0.0	0.8	
	b_6	−1.6	−0.8	−0.2	1.1	1.0	
	b_7	0.3	0.4	0.0	0.4	−0.8	
	b_8	−0.6	−1.0	−0.2	−0.9	0.6	
H	Φ						0.7
	h_1						1.5
	h_2						0.7
	h_3						−0.6
	h_4						−0.8
	h_5						1.5

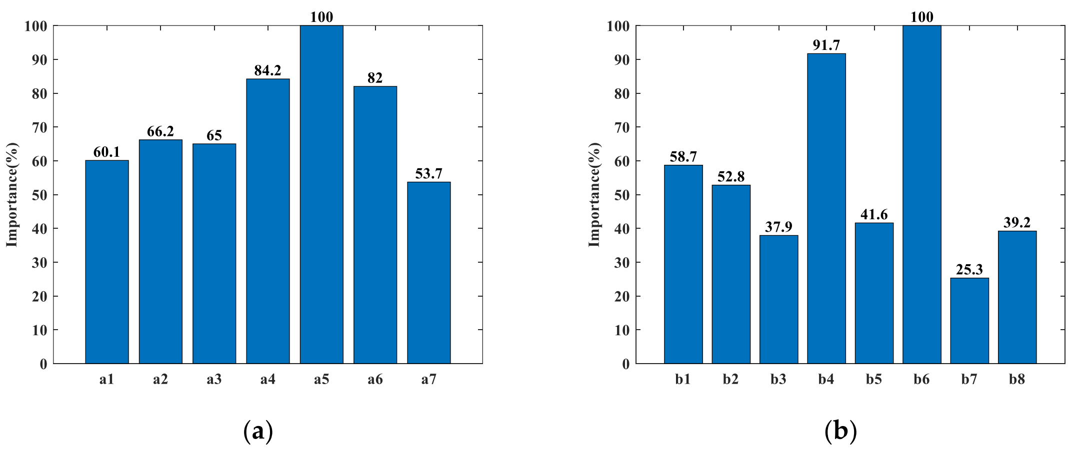

Figure 10. Importance of parameters. (**a**) PE debonding; (**b**) IC debonding.

From Figure 10, it can be seen that for PE debonding, the degree of influence of each parameter on the output result is a5, a4, a6, a2, a3, a1, a7; for IC debonding, the degree of influence of each indicator on the output is b6, b4, b1, b2, b5, b8, b3, b7.

6. Discussion and Conclusions

Researchers have proposed different prediction models for PE and IC debonding and these models for predicting PE and IC debonding have facilitated the study of the debonding failure of FRP-strengthened RC beams. Still, they have significant coefficients of variation between the calculated and experimental values.

This paper used correlation analysis and grey correlation analysis to construct the indicator system for debonding failure. PE and IC debonding prediction models for FRP-strengthened RC beams were developed by several machine learning algorithms. Optimization of the model took place using the Dung Beetle Optimizer and comparison with the model suggested by codes. We can draw the following conclusions:

(1) The correlation between the indicators in the established mixed indicator system is insignificant, and the correlation with the predicted values is significant. Additionally, FRP stiffness (Eftf) and concrete strength (f'c) have a large effect on both PE and IC debonding.
(2) For the prediction of PE and IC debonding, the BP neural network has the best performance compared to other machine learning algorithms.
(3) The model optimized by the DBO algorithm is significantly accurate and can better predict PE and IC debonding. The models suggested by codes have a significant coefficient of variation and are conservative or overestimate the state of the strengthened beam in case of failure.
(4) The experimental data used in this paper are unevenly distributed, which will affect the accuracy of the model to some extent. More data need to be collected in the future to build a more reliable model. Additionally, the parameters considered in this paper are not complete and more parameters need to be investigated in the future.

Author Contributions: Conceptualization, methodology, software, validation, writing—original draft, writing, T.H.; supervision, funding acquisition, writing, H.Z.; funding acquisition, supervision, J.Z. All authors have read and agreed to the published version of the manuscript.

Funding: This study was supported by the National Natural Science Foundation of China (52278291), and the Chongqing Natural Science Foundation of China (CSTB2022NSCQ-LZX0006, cstc2020jcyj-jqX0006, cstc2022ycjh-bgzxm0086).

Data Availability Statement: Not applicable.

Conflicts of Interest: The authors declare no conflict of interest.

References

1. Li, S.; Xin, J.; Jiang, Y.; Wang, C.; Zhou, J.; Yang, X. Temperature-induced deflection separation based on bridge deflection data using the TVFEMD-PE-KLD method. *J. Civ. Struct. Health Monit.* **2023**, 1–17. [CrossRef]
2. Jiang, Y.; Hui, Y.; Wang, Y.; Peng, L.; Huang, G.; Liu, S. A novel eigenvalue-based iterative simulation method for multi-dimensional homogeneous non-Gaussian stochastic vector fields. *Struct. Saf.* **2023**, *100*, 102290. [CrossRef]
3. Zhang, H.; Li, H.; Zhou, J.; Tong, K.; Xia, R. A multi-dimensional evaluation of wire breakage in bridge cable based on self-magnetic flux leakage signals. *J. Magn. Magn. Mater.* **2023**, *566*, 170321. [CrossRef]
4. Xin, J.; Jiang, Y.; Zhou, J.; Peng, L.; Liu, S.; Tang, Q. Bridge deformation prediction based on SHM data using improved VMD and conditional KDE. *Eng. Struct.* **2022**, *261*, 114285. [CrossRef]
5. Kotynia, R.; Oller, E.; Marí, A.; Kaszubska, M. Efficiency of shear strengthening of RC beams with externally bonded FRP materials—State-of-the-art in the experimental tests. *Compos. Struct.* **2021**, *267*, 113891. [CrossRef]
6. Bakay, R.; Sayed-Ahmed, E.Y.; Shrive, N.G. Interfacial debonding failure for reinforced concrete beams strengthened with carbon-fibre-reinforced polymer strips. *Can. J. Civ. Eng.* **2009**, *36*, 103–121. [CrossRef]
7. Ceroni, F.; Pecce, M.; Matthys, S.; Taerwe, L. Debonding strength and anchorage devices for reinforced concrete elements strengthened with FRP sheets. *Compos. Part B Eng.* **2008**, *39*, 429–441. [CrossRef]

8. Al-Saawani, M.A.; El-Sayed, A.K.; Al-Negheimish, A.I. Assessment of plate-end debonding design provisions for RC beams strengthened with FRP. *Lat. Am. J. Solids Struct.* **2020**, *17*. [CrossRef]
9. Chen, J.; Sun, B.; Bao, Z. A brief discussion of the prestressed carbon fiber board reinforcement material system. In Proceedings of the Twelfth National Academic Exchange Conference on Building Inspection, Appraisal and Reinforcement, Guangzhou, China, 6–7 December 2004.
10. Al-Saawani, M.; El-Sayed, A.K.; Al-Negheimish, A.I. Effect of basic design parameters on IC debonding of CFRP-strengthened shallow RC beams. *J. Reinf. Plast. Compos.* **2015**, *34*, 1526–1539. [CrossRef]
11. Oehlers, D.J. Reinforced Concrete Beams with Plates Glued to their Soffits. *J. Struct. Eng.* **1992**, *118*, 2023–2038. [CrossRef]
12. Zhang, S.-S.; Teng, J.G. End cover separation in RC beams strengthened in flexure with bonded FRP reinforcement: Simplified finite element approach. *Mater. Struct.* **2015**, *49*, 2223–2236. [CrossRef]
13. Jansze, W. Strengthening of RC Members in Bending by Externally Bonded Steel Plates. Ph.D. Thesis, Delft University of Technology, Delft, The Netherlands, 1997.
14. Ahmed, O.; Van Gemert, D. Effect of Longitudinal Carbon Fiber Reinforced Plastic Laminates on Shear Capacity of Reinforced Concrete Beams. *Spec. Publ.* **1999**, *188*, 933–944. [CrossRef]
15. FIB International. *Externally Applied FRP Reinforcement for Concrete Structures*; FIB International: Lausanne, Switzerland, 2001.
16. Smith, S.; Teng, J. FRP-strengthened RC beams. II: Assessment of debonding strength models. *Eng. Struct.* **2002**, *24*, 397–417. [CrossRef]
17. Yao, J.; Teng, J. Plate end debonding in FRP-plated RC beams—I: Experiments. *Eng. Struct.* **2007**, *29*, 2457–2471. [CrossRef]
18. Concrete Society. *Design Guidance for Strengthening Concrete Structures Using Fibre Composite Materials*, 2nd ed.; Concrete Society Technical Rep. 55; Concrete Society: Surrey, UK, 2004.
19. American Concrete Institute Committee. *440 Report. Guide for the Design and Construction of Externally Bonded FRP Systems for Strengthening Concrete Structures*; American Concrete Institute Committee: Farmington Hills, MI, USA, 2017.
20. *AS 5100.8*; Bridge Design, Part 8: Rehabilitation and Strengthening of Existing Bridges. Standards Australia, SA1 Global Limited: Sydney, Austrilia, 2017.
21. El-Sayed, A.K.; Al-Saawani, M.A.; Al-Negheimish, A.I. Empirical shear based model for predicting plate end debonding in FRP strengthened RC beams. *J. Civ. Eng. Manag.* **2021**, *27*, 117–138. [CrossRef]
22. Japan Society of Civil Engineers (JSCE). *Recommendations for Upgrading of Concrete Structures with Use of Continuous Fiber Sheets*; Japan Society of Civil Engineers (JSCE): Tokyo, Japan, 1997.
23. China Association for Engineering Construction Standardization (CECS146). *Technical Specification for Strengthening Concrete Structure with Carbon Fiber Reinforced Polymer Laminate*; China Planning Press: Beijing, China, 2003.
24. *CNR-DT, 200*; Guide for the Design and Construction of Externally Bonded FRP Systems for Strengthening Existing Structures. Italian National Research Council: Rome, Italy, 2004.
25. Kim, Y.J.; Harries, K.A. Statistical Characterization of Reinforced Concrete Beams Strengthened with FRP Sheets. *J. Compos. Constr.* **2013**, *17*, 357–370. [CrossRef]
26. Bilotta, A.; Faella, C.; Martinelli, E.; Nigro, E. Design by testing procedure for intermediate debonding in EBR FRP strengthened RC beams. *Eng. Struct.* **2013**, *46*, 147–154. [CrossRef]
27. López-González, J.C.; Fernández-Gómez, J.; Díaz-Heredia, E.; López-Agüí, J.C.; Villanueva-Llauradó, P. IC debonding failure in RC beams strengthened with FRP: Strain-based versus stress increment-based models. *Eng. Struct.* **2016**, *118*, 108–124. [CrossRef]
28. Li, X.-H.; Wu, G. Finite-Element Analysis and Strength Model for IC Debonding in FRP-Strengthened RC Beams. *J. Compos. Constr.* **2018**, *22*, 04018030. [CrossRef]
29. Zhang, J.; Guo, R.; Li, S.; Zhao, S. Prediction of the IC debonding failure of FRP-strengthened RC beams based on the cohesive zone model. *Lat. Am. J. Solids Struct.* **2020**, *17*. [CrossRef]
30. Fang, Z.; Roy, K.; Chen, B.; Sham, C.-W.; Hajirasouliha, I.; Lim, J.B. Deep learning-based procedure for structural design of cold-formed steel channel sections with edge-stiffened and un-stiffened holes under axial compression. *Thin-Walled Struct.* **2021**, *166*, 108076. [CrossRef]
31. Fang, Z.; Roy, K.; Ingham, J.; Lim, J.B.P. Assessment of end-two-flange web crippling strength of roll-formed aluminium alloy perforated channels by experimental testing, numerical simulation, and deep learning. *Eng. Struct.* **2022**, *268*, 114753. [CrossRef]
32. Fang, Z.; Roy, K.; Xu, J.; Dai, Y.; Paul, B.; Lim, J.B. A novel machine learning method to investigate the web crippling behaviour of perforated roll-formed aluminium alloy unlipped channels under interior-two flange loading. *J. Build. Eng.* **2022**, *51*, 104261. [CrossRef]
33. Ritchie, P.A.; Thomas, D.A.; Lu, L.W.; Conelly, G.M. External reinforcement of concrete beams using fibre reinforced plastics. *ACI Struct. J.* **1991**, *88*, 490–500.
34. Quantrill, R.J.; Hollaway, L.C.; Thorne, A.M. Experimental and analytical investigation of FRP strengthened beam response: Part I. *Mag. Concr. Res.* **1996**, *48*, 331–342. [CrossRef]
35. Arduini, M.; Di Tommaso, A.; Nanni, A. Brittle failure in FRP plate and sheet bonded beams. *ACI Struct. J.* **1997**, *94*, 363–370.
36. Garden, H.N.; Hollaway, L.C.; Thorne, A.M. A preliminary evaluation of carbon fibre reinforced polymer plates for strengthening reinforced concrete members. *Proc. Inst. Civ. Eng. Struct. Build.* **1997**, *123*, 127–142. [CrossRef]
37. Garden, H.N.; Quantrill, R.J.; Hollaway, L.C.; Thorne, A.M.; Parke, G.A.R. An experimental study of the anchorage length of carbon fiber composite plates used to strengthen reinforced concrete beams. *Constr. Build. Mater.* **1998**, *12*, 203–219. [CrossRef]

38. Beber, A.J.; Campos Filho, A.; Campagnolo, J.L. Flexural strengthening of R/C beams with CFRP sheets. In Proceedings of the 8th International Conference in Structural Faults - Repair-99, London, UK, 13–15 July 1999.
39. David, E.; Djelal, C.; Ragneau, E.; Bodin, F.B. Use of FRP to strengthen and repair RC beams: Experimental study and numerical simulations. In Proceedings of the Eighth International Conference on Advanced Composites for Concrete Repair, London, UK, 1999.
40. Hau, K.M. Experiments on Concrete Beams Strengthened by Bonding Fibre Reinforced Plastic Sheets. Master's Thesis, The Hong Kong Polytechnic University, Hong Kong, China, 1999.
41. Tumialan, G.; Serra, P.; Nanni, A.; Belarbi, A. Concrete cover delamination in reinforced concrete beams strengthened with carbon fiber reinforced polymer sheets. In Proceedings of the Fourth International Symposium on Fiber Reinforced Polymer Reinforcement for Reinforced Concrete Structures, Baltimore, MD, USA, 1 January 1999; pp. 725–735.
42. Ahmed, O.A.F. Strengthening of R. C. Beams by Means of Externally bonded CFRP Laminates: Improved Model for Plateend shear. Ph.D. Thesis, Department of Civil Engineering, Catholicke University of Leuven, Leuven, Belgium, 2000.
43. Matthys, S. Structural Behavior and Design of Concrete Beams Strengthened with Externally Bonded FRP Reinforcement. Ph.D. Thesis, Ghent University, Ghent, Belgium, 2000.
44. Fanning, P.J.; Kelly, O. Ultimate Response of RC Beams Strengthened with CFRP Plates. *J. Compos. Constr.* **2001**, *5*, 122–127. [CrossRef]
45. Gao, B.; Leung, W.; Cheung, C.; Kim, J.K.; Leung, C.K.Y. Effects of adhesive properties on strengthening of concrete beams with composite strips. In Proceedings of the International Conference on FRP Composites in Civil Engineering, Hong Kong, China, 12–15 December 2001; pp. 423–432.
46. Maalej, M.; Bian, Y. Interfacial shear stress concentration in FRP-strengthened beams. *Compos. Struct.* **2001**, *54*, 417–426. [CrossRef]
47. Nguyen, D.M.; Chan, T.K.; Cheong, H.K. Brittle Failure and Bond Development Length of CFRP-Concrete Beams. *J. Compos. Constr.* **2001**, *5*, 12–17. [CrossRef]
48. Rahimi, H.; Hutchinson, A. Concrete Beams Strengthened with Externally Bonded FRP Plates. *J. Compos. Constr.* **2001**, *5*, 44–56. [CrossRef]
49. Smith, S.; Teng, J.G. Shear-Bending Interaction in Debonding Failures of FRP-Plated RC Beams. *Adv. Struct. Eng.* **2003**, *6*, 183–199. [CrossRef]
50. Valcuende, M.; Benlloch, J.; Parra, C.J. Ductility of reinforced concrete beams strengthened with CFRP strips and fabric. In Proceedings of the Sixth International Symposium on FRP Reinforcement for Concrete Structures, Singapore, 8–10 July 2003; pp. 337–346.
51. Breña, S.F.; Macri, B.M. Effect of Carbon-Fiber-Reinforced Polymer Laminate Configuration on the Behavior of Strengthened Reinforced Concrete Beams. *J. Compos. Constr.* **2004**, *8*, 229–240. [CrossRef]
52. Gao, B.; Kim, J.K.; Leung, C.K.Y. Taper ended FRP strips bonded to RC beams: Experiments and FEM analysis. In Proceedings of the Second International Conference on FRP in Civil Engineering, Adelaide, Australia, 8–10 December 2004; pp. 399–405.
53. Gao, B.; Kim, J.-K.; Leung, C.K. Experimental study on RC beams with FRP strips bonded with rubber modified resins. *Compos. Sci. Technol.* **2004**, *64*, 2557–2564. [CrossRef]
54. Grace, N.F.; Singh, S.B. Durability evaluation of carbon fiber-reinforced polymer strengthened concrete beams: Experimental study and design. *ACI Struct. J.* **2005**, *102*, 40–48.
55. Pham, H.B.; Al-Mahaidi, R. Prediction algorithms for debonding failure loads of carbon fiber reinforced polymer retrofitted reinforced concrete beams. *J. Compos. Constr.* **2006**, *10*, 48–59. [CrossRef]
56. Benjeddou, O.; Ben Ouezdou, M.; Bedday, A. Damaged RC beams repaired by bonding of CFRP laminates. *Constr. Build. Mater.* **2007**, *21*, 1301–1310. [CrossRef]
57. Esfahani, M.R.; Kianoush, M.R.; Tajari, A.R. Flexural behavior of reinforced concrete beams strengthened by CFRP sheets. *Eng. Struct.* **2007**, *29*, 2428–2444. [CrossRef]
58. Ceroni, F. Experimental performances of RC beams strengthened with FRP materials. *Constr. Build. Mater.* **2010**, *24*, 1547–1559. [CrossRef]
59. Al-Tamimi, A.K.; Hawileh, R.; Abdalla, J.; Rasheed, H.A. Effects of Ratio of CFRP Plate Length to Shear Span and End Anchorage on Flexural Behavior of SCC RC Beams. *J. Compos. Constr.* **2011**, *15*, 908–919. [CrossRef]
60. Sadrmomtazi, A.; Rasmi Atigh, H.; Sobhan, J. Experimental and analytical investigation on bond performance of the interfacial debonding in flexural strengthened RC beams with CFRP sheets at tensile face. *Asian J. Civ. Eng. (BHRC)* **2014**, *15*, 391–410.
61. Hasnat, A.; Islam, M.M.; Amin, A.F.M.S. Enhancing the Debonding Strain Limit for CFRP-Strengthened RC Beams Using U-Clamps: Identification of Design Parameters. *J. Compos. Constr.* **2016**, *20*. [CrossRef]
62. Skuturna, T.; Valivonis, J. Experimental study on the effect of anchorage systems on RC beams strengthened using FRP. *Compos. Part B Eng.* **2016**, *91*, 283–290. [CrossRef]
63. Saadatmanesh, H.; Ehsani, M.R. RC beams strengthened with GFRP plates. I: Experimental study. *J. Struct. Eng.* **1991**, *117*, 3417–3433. [CrossRef]
64. Arduini, M.; Nanni, A. Behavior of Precracked RC Beams Strengthened with Carbon FRP Sheets. *J. Compos. Constr.* **1997**, *1*, 63–70. [CrossRef]
65. Spadea, G.; Swamy, R.N.; Bencardino, F. Strength and Ductility of RC Beams Repaired with Bonded CFRP Laminates. *J. Bridg. Eng.* **2001**, *6*, 349–355. [CrossRef]

66. White, T.W.; Soudki, K.A.; Erki, M.-A. Response of RC Beams Strengthened with CFRP Laminates and Subjected to a High Rate of Loading. *J. Compos. Constr.* **2001**, *5*, 153–162. [CrossRef]
67. Grace, N.F.; Abdel-Sayed, G.; Ragheb, W. Strengthening of concrete beams using innovative ductile fiber-reinforced polymer fabric. *Struct. J.* **2002**, *99*, 692–700.
68. Alagusundaramoorthy, P.; Harik, I.E.; Choo, C.C. Flexural Behavior of R/C Beams Strengthened with Carbon Fiber Reinforced Polymer Sheets or Fabric. *J. Compos. Constr.* **2003**, *7*, 292–301. [CrossRef]
69. Maalej, M.; Leong, K. Effect of beam size and FRP thickness on interfacial shear stress concentration and failure mode of FRP-strengthened beams. *Compos. Sci. Technol.* **2005**, *65*, 1148–1158. [CrossRef]
70. Zhang, A.-H.; Jin, W.-L.; Li, G.-B. Behavior of preloaded RC beams strengthened with CFRP laminates. *J. Zhejiang Univ. A* **2006**, *7*, 436–444. [CrossRef]
71. Lee, S.; Moy, S. A Method for Predicting the Flexural Strength of RC Beams Strengthened with Carbon Fiber Reinforced Polymer. *J. Reinf. Plast. Compos.* **2007**, *26*, 1383–1401. [CrossRef]
72. Rusinowski, P.; Täljsten, B. Intermediate Crack Induced Debonding in Concrete Beams Strengthened with CFRP Plates—An Experimental Study. *Adv. Struct. Eng.* **2009**, *12*, 793–806. [CrossRef]
73. Gunes, O.; Buyukozturk, O.; Karaca, E. A fracture-based model for FRP debonding in strengthened beams. *Eng. Fract. Mech.* **2009**, *76*, 1897–1909. [CrossRef]
74. Pan, J.; Leung, C.K.; Luo, M. Effect of multiple secondary cracks on FRP debonding from the substrate of reinforced concrete beams. *Constr. Build. Mater.* **2010**, *24*, 2507–2516. [CrossRef]
75. Sena-Cruz, J.M.; Barros, J.A.; Coelho, M.R.; Silva, L.F. Efficiency of different techniques in flexural strengthening of RC beams under monotonic and fatigue loading. *Constr. Build. Mater.* **2012**, *29*, 175–182. [CrossRef]
76. Kotynia, R. Debonding failures of RC beams strengthened with externally bonded strips. In Proceedings of the International Symposium on Bond Behaviour of FRP in Structures (BBFS 2005), Hong Kong, China, 7–9 December 2005.
77. Al-Zaid, R.A.; El-Sayed, A.K.; Al-Negheimish, A.I.; Shuraim, A.B.; Alhozaimy, A.M. Strengthening of structurally damaged wide shallow RC beams using externally bonded CFRP plates. *Lat. Am. J. Solids Struct.* **2014**, *11*, 946–965. [CrossRef]
78. Yalim, B.; Kalayci, A.S.; Mirmiran, A. Performance of FRP-Strengthened RC Beams with Different Concrete Surface Profiles. *J. Compos. Constr.* **2008**, *12*, 626–634. [CrossRef]
79. Bi, Y.; Wu, S.; Pei, J.; Wen, Y.; Li, R. Correlation analysis between aging behavior and rheological indices of asphalt binder. *Constr. Build. Mater.* **2020**, *264*, 120176. [CrossRef]
80. Kong, L.; Chen, X.; Du, Y. Evaluation of the effect of aggregate on concrete permeability using grey correlation analysis and ANN. *Comput. Concr.* **2016**, *17*, 613–628. [CrossRef]
81. Huang, C.-H.; Hsieh, S.-H. Predicting BIM labor cost with random forest and simple linear regression. *Autom. Constr.* **2020**, *118*, 103280. [CrossRef]
82. Wang, X.; Liang, Y.; Wang, Q.; Zhang, Z. Empirical models for tool forces prediction of drag-typed picks based on principal component regression and ridge regression methods. *Tunn. Undergr. Space Technol.* **2017**, *62*, 75–95. [CrossRef]
83. Dabiri, H.; Farhangi, V.; Moradi, M.J.; Zadehmohamad, M.; Karakouzian, M. Applications of Decision Tree and Random Forest as Tree-Based Machine Learning Techniques for Analyzing the Ultimate Strain of Spliced and Non-Spliced Reinforcement Bars. *Appl. Sci.* **2022**, *12*, 4851. [CrossRef]
84. Moradi, N.; Tavana, M.H.; Habibi, M.R.; Amiri, M.; Moradi, M.J.; Farhangi, V. Predicting the Compressive Strength of Concrete Containing Binary Supplementary Cementitious Material Using Machine Learning Approach. *Materials* **2022**, *15*, 5336. [CrossRef]
85. Xue, J.; Shen, B. Dung beetle optimizer: A new meta-heuristic algorithm for global optimization. *J. Supercomput.* **2022**, 1–32. [CrossRef]